Communication

Chelator PBT2 forms a ternary Cu^{2+} complex with β-amyloid that has high stability but low specificity

Simon Drew [1,2,*]

[1] Institut Pasteur, Université Paris Cité, Inserm U1224, F-75015, Paris, France; sdrew@pasteur.fr
[2] Department of Medicine (Royal Melbourne Hospital), The University of Melbourne, Victoria 3010, Australia; sdrew@unimelb.edu.au
* Correspondence: sdrew@unimelb.edu.au

Abstract: The metal chelator PBT2 (5,7-dichloro-2-[(dimethylamino)methyl]-8-hydroxyquinoline) acts as a terdentate ligand capable of forming binary and ternary Cu^{2+} complexes. It was clinically trialed as an Alzheimer's disease (AD) therapeutic but failed to progress beyond phase II. The β-amyloid (Aβ) peptide associated with AD was recently concluded to form a unique Cu(Aβ) complex that is inaccessible to PBT2. Herein, it is shown that the species ascribed to this binary Cu(Aβ) complex in fact corresponds to ternary $Cu(PBT2)N_{Im}^{A\beta}$ complexes formed by anchoring of Cu(PBT2) on imine nitrogen (N_{Im}) donors of His side chains. The primary site of ternary complex formation is His6, having a conditional stepwise formation constant at pH 7.4 (${}^{c}K$ [M^{-1}]) of log ${}^{c}K$ = 6.4 ± 0.1, and a second site is supplied by His13 or His14 (log ${}^{c}K$ = 4.4 ± 0.1). The stability of $Cu(PBT2)N_{Im}^{H13/14}$ is comparable with that of the simplest ternary complexes involving free imidazole (log ${}^{c}K$ = 4.22 ± 0.09) and histamine (log ${}^{c}K$ = 4.00 ± 0.05). The 100-fold larger formation constant for $Cu(PBT2)N_{Im}^{H6}$ indicates that outer-sphere ligand–peptide interactions strongly stabilize its structure. Despite the relatively high stability of $Cu(PBT2)N_{Im}^{H6}$, PBT2 is a promiscuous Cu^{2+}-binding ligand capable of forming a ternary $Cu(PBT2)N_{Im}$ complex with any ligand containing N_{Im} donor. These ligands include histamine, L-His, and ubiquitous His side chains of peptides and proteins in the extracellular milieu, whose combined effect should outweigh that of a single $Cu(PBT2)N_{Im}^{H6}$ complex regardless of its stability. We therefore conclude that PBT2 is capable of accessing Cu(Aβ) complexes with high stability but not specificity. The results have implications for future AD therapeutic strategies and understanding the role of PBT2 in the bulk transport of transition metal ions. Given the repurposing of PBT2 as a drug for breaking antibiotic resistance, ternary $Cu(PBT2)N_{Im}$ and analogous $Zn(PBT2)N_{Im}$ complexes may be relevant to its antimicrobial properties.

Keywords: 8-hydroxyquinoline; PBT2; amyloid; copper; ternary; terdentate; antimicrobial

1. Introduction

The compound 5,7-dichloro-2-[(dimethylamino)methyl]-8-hydroxyquinoline (PBT2) is a terdentate Cu^{2+} and Zn^{2+} chelator that was previously trialled as a therapeutic to treat Alzheimer's disease (AD). Its anticipated mechanism of action was based on the controversial "metals hypothesis", which proposed that AD results from aberrant interactions of the β-amyloid (Aβ) peptide with endogenous transition metal ions, notably Cu^{2+}, causing Aβ to misfold and generate reactive oxygen species (ROS) [1,2]. PBT2 was proposed to prevent these interactions, sequester transition metal ions thought to be trapped within extracellular β-amyloid aggregates, and then enable cellular uptake of these ions by ionophore action [3]. However, repeated phase II clinical trials ultimately provided no evidence for cognitive efficacy of PBT2 in patients with prodromal or mild AD [4,5].

Using electron paramagnetic resonance (EPR) spectroscopy, the Cu^{2+} coordination of this class of ligand (L) was first characterized using the non-chlorinated homologue of PBT2 (Figure 1), which was shown to form a terdentate CuL complex and a five-coordinate CuL_2 complex [6]. The proposed structure of CuL_2 has been replicated in the crystal structure of PBT2 [7], and the UV-vis and EPR spectroscopic properties of Cu(PBT2) and $Cu(PBT2)_2$ have been shown to mirror those of the non-chlorinated homologue [6,7,8,9] (Table S1). Early EPR studies also showed that both ligands form ternary $CuLN_{Im}^{X}$ complexes (Figure 1) in which the labile Cl^- ligand

Preprints (www.preprints.org) | NOT PEER-REVIEWED | Posted: 5 May 2023 doi:10.20944/preprints202305.0275.v1

of CuL is replaced with an imine (N_{Im}) donor ligand provided by X = imidazole, histamine, L-His, or proteins such as α-synuclein and Aβ (see, in particular, Figure S33 of ref. [6]). However, despite recently identifying a similar EPR spectroscopic signature using a Cu/PBT2/$A\beta_{1-42}$ mixture, George and coworkers ascribed the signal to a unique PBT2-inaccessible Cu(Aβ) species and concluded that there was no evidence to support formation of a ternary Cu^{2+} complex [10]. Since this could be interpreted by some as a reason for the failure of PBT2 in AD clinical trials, it is important to resolve this contradiction.

To address the above issue, we used EPR spectroscopy to analyze the species distributions in Cu/PBT2/Aβ mixtures in unprecedented detail. We identified ternary Cu(PBT2)N_{Im}^{X} complex formation with X = His6 and His13/14 of $A\beta_{1-40}$ and derived the corresponding stepwise conditional formation constants at pH 7.4. For comparison, we also determined the conditional formation constants for X = imidazole and histamine using PBT2 and its non-chlorinated homologue. The stepwise conditional formation constant for Cu(PBT2)N_{Im}^{H6} was found to be 3.5-fold larger than that for $Cu(PBT2)_2$ at pH 7.4 and 100-fold larger than the stepwise formation constants for Cu(PBT2)$N_{Im}^{H13/14}$ and Cu(PBT2)N_{Im}^{X} (X = imidazole, histamine).

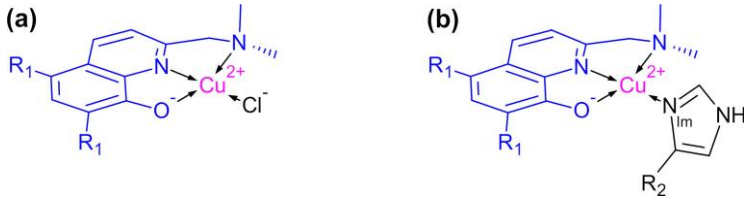

Figure 1. Structure of **(a)** binary and **(b)** ternary Cu^{2+} complexes of PBT2 (R_1 = Cl) and its non-chlorinated homologue (R_1 = H). The imine nitrogen (N_{Im}) is supplied by ligands including imidazole (R_2 = H), histamine ($R_2 = CH_2CH_2NH_3^+$), L-His ($R_2 = CH_2(COO^-)CHNH_3^+$), and His side chains ($R_2$ = protein).

2. Results

To characterize the Cu^{2+} complexes formed by PBT2 in the presence of Aβ, we titrated Cu^{2+} into an equimolar mixture of PBT2 and $A\beta_{1-40}$ in PBS pH 7.4 and acquired the corresponding EPR spectra (Figure 2a). To determine the species distribution, each spectrum was decomposed into a linear superposition of basis spectra (Figure 2b) corresponding to Cu(PBT2), $Cu(PBT2)_2$, Cu($A\beta_{1-40}$), $Cu_2(A\beta_{1-40})$, and the putative Cu(PBT2)$N_{Im}^{A\beta}$ complex. The spectrum of Cu(PBT2) was obtained at equimolar Cu/PBT2 stoichiometry and that of $Cu(PBT2)_2$ at sub-stoichiometric ratios (Figure S1). The spectra of Cu(Aβ) and Cu_2(Aβ) were acquired at Cu/Aβ ratios of 1:1 and 2.5:1 (Figure S2). Attempts to use linear combinations of normalized Cu(PBT2), $Cu(PBT2)_2$, Cu(Aβ), and Cu_2(Aβ) spectra failed to reproduce the EPR spectra of Cu/PBT2/$A\beta_{1-40}$ n:1:1 (n = 0–2.67), indicating that additional species must be formed. Indeed, the dominant spectral features did not resemble any of those of the above four species (Figure 2b; Figure S3). Rather, they corresponded closely to those of previously characterized CuLN_{Im} complexes (Table 1) [6,8,11], indicating that Cu(PBT2) can anchor on the imine nitrogen (N_{Im}) of the His side chains of $A\beta_{1-40}$.

To quantify the number and stabilities of ternary Cu(PBT2)$N_{Im}^{A\beta}$ interactions, it is important to consider how the His residues participate in binary Cu(Aβ) complexes. At pH 7.4, Cu(Aβ) is dominated by {NH_2^{D1}, $C{=}O^{D1}$, N_{Im}^{H6}, N_{Im}^{H13}} and {NH_2^{D1}, $C{=}O^{D1}$, N_{Im}^{H6}, N_{Im}^{H14}} coordination spheres with indistinguishable EPR spectra [12,13,14]. Thus, His6 is absolutely required to form Cu(Aβ), whereas only one of His13 or His14 is needed. Thus, anchoring of Cu(PBT2) on His6 to form Cu(PBT2)N_{Im}^{H6} will occur at the expense of Cu(Aβ), whereas anchoring on one of His13 or His14 to form Cu(PBT2)$N_{Im}^{H13/14}$ will not. Sequential binding of a second Cu^{2+} ion by Cu(Aβ) generates Cu_2(Aβ). The coordination in Cu_2(Aβ) remains poorly defined, with one suggestion that sequential binding of a second Cu^{2+} ion changes the coordination of the first [15]. However, it will be shown below that a satisfactory explanation of the species distributions requires that His6 remains Cu^{2+}-bound and His13 or His14 non-coordinated in Cu_2(Aβ).

Preprints (www.preprints.org) | NOT PEER-REVIEWED | Posted: 5 May 2023 doi:10.20944/preprints202305.0275.v1

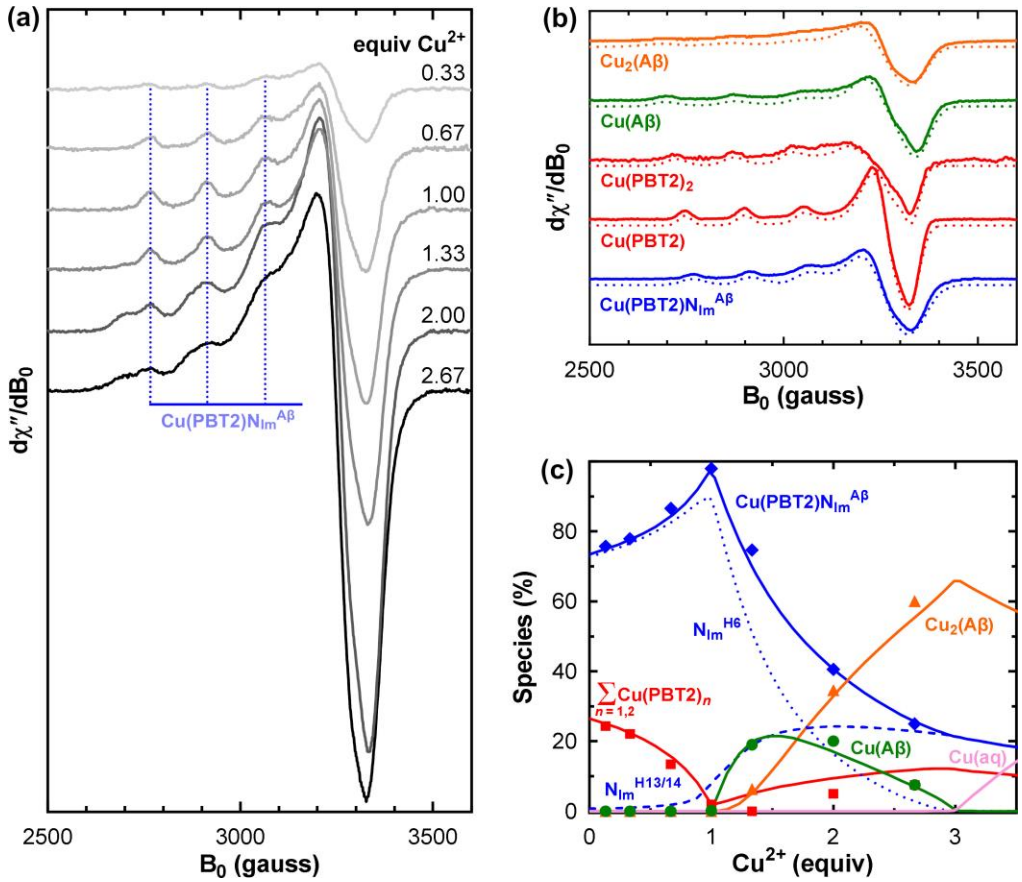

Figure 2. Determination of the number and stabilities of ternary Cu(PBT2)(Aβ$_{1–40}$) interactions. (**a**) EPR spectra of ^{65}Cu/PBT2/Aβ$_{1–40}$ *n*:1:1 (*n* = 0.1–2.67) in PBS pH 7.4 (0.2 mM PBT2/Aβ$_{1–40}$). **(b)** Normalized basis set used for the decomposition of the spectra in panel *a* (see Figures S1–S3 for details). Dotted lines show spectra simulated using the parameters in Table 1. The Cu$_2$Aβ$_{1–40}$ simulation comprised spectra using "first site" parameters (50%) and "second site" parameters (50%). Vertical scales in panels *a* and *b* are different. **(c)** Experimental species distributions (points) resulting from normalisation and decomposition of the spectra in panel *a* (Figure S4), and theoretical distributions (lines) calculated using the relevant formation constants in Table 2 (see also Figure S5 for a comparison of relative and absolute Cu^{2+} speciation). The solid blue line in panel *c* shows the sum of the Cu(PBT2)N$_{Im}^{H6}$ (dotted line) and Cu(PBT2)N$_{Im}^{H13/14}$ (dashed line). Cu(aq) denotes aqueous Cu^{2+} (pink). Experimental conditions: temperature, 77 K; microwave power, 10 mW; microwave frequency, 9.425 GHz; modulation amplitude, 8 G; sweep time, 84 s; time constant, 82 ms; averages, 4.

The conditional constants (^cK) for formation of Cu(PBT2), Cu(PBT2)$_2$, Cu(Aβ), and Cu$_2$(Aβ) at pH 7.4 have all been previously determined (Table S2), which greatly simplified the task of determining the species distribution of the Cu/PBT2/Aβ$_{1–40}$ *n*:1:1 system. Using these values and the EPR basis spectra (Figure 2b), we fitted the series of EPR spectra in Figure 2a as a function of the unknown constants $^cK^{CuL}_{CuLN_{Im}^{H6}}$ and $^cK^{CuL}_{CuLN_{Im}^{H13/14}}$ (see Section 4.3 for detail). The best agreement between the experimental and theoretical species distributions (Figure 2c) was obtained for log $^cK^{CuL}_{CuLN_{Im}^{H6}}$ = 6.4 ± 0.1 and log $^cK^{CuL}_{CuLN_{Im}^{H13/14}}$ = 4.4 ± 0.1 (Table 2). Allowing the conditional formation constants $^cK^{Cu}_{Cu(A\beta)}$ and $^cK^{Cu(A\beta)}_{Cu_2(A\beta)}$ to vary beyond their generally accepted ranges worsened the fit. Although we did not refine the value of $^cK^{CuL}_{CuL_2}$, we found that large changes from its published value also worsened the fit unless $^cK^{Cu}_{Cu(A\beta)}$ was set to a value beyond its accepted range.

The general appearance of the species distributions for Cu/PBT2/Aβ$_{1–40}$ *n*:1:1 (Figure 2c, Figure S5) can be understood as follows. For small *n*, the 1000-fold greater stability of Cu(PBT2) compared with Cu(Aβ) (Table 2) ensures that Cu^{2+} will first bind to PBT2, with the identity of the fourth in-plane ligand then being determined by the relative magnitudes of the stepwise constants $^cK^{CuL}_{CuLN_{Im}^{H6}} > {}^cK^{CuL}_{CuL_2} \gg {}^cK^{CuL}_{CuLN_{Im}^{H13/14}}$. Thus, for $n < 1$, Cu^{2+} is

Preprints (www.preprints.org) | NOT PEER-REVIEWED | Posted: 5 May 2023 doi:10.20944/preprints202305.0275.v1

predominantly bound in a Cu(PBT2)N_{Im}^{H6} complex with a minor quantity of Cu(PBT2)$_2$. For n = 1, Cu(PBT2)$_2$ is almost entirely replaced by Cu(PBT2)N_{Im}^{H6} and Cu(PBT2)$N_{Im}^{H13/14}$, which only require one PBT2 molecule per Cu^{2+} ion. For n > 1, with no free PBT2 molecules available, the additional Cu^{2+} is coordinated in the next most stable binary complex, which is Cu(Aβ) ($\log {}^{c}K^{Cu}_{Cu(A\beta)} = 10.0 \pm 0.1$). However, because Cu(Aβ) coordination requires His6, some Cu(PBT2) detaches from His6 and anchors instead on a His13 or His14 side chain, albeit with lower stability, to form Cu(PBT2)$N_{Im}^{H13/14}$. As the available sites at His6 are gradually filled by Cu(Aβ), stepwise addition of a second Cu^{2+} ion to the peptide occurs ($\log {}^{c}K^{Cu(A\beta)}_{Cu_2(A\beta)} = 8.0 \pm 0.1$) to form Cu$_2$(Aβ). Maximum occupancy of the Cu/PBT2/Aβ$_{1–40}$ n:1:1 system is reached at n = 3, with two Cu^{2+} ions are bound to the "first" and "second" sites of Aβ, and a third Cu^{2+} ion bound either to Cu(PBT2) that is free (minor) or anchored to His13/14 of Cu$_2$(Aβ) in a Cu(PBT2)$N_{Im}^{H13/14}$ complex (major).

Table 1. Principal electron Zeeman (g_z) and nuclear hyperfine (A_z) parameters of binary and ternary Cu^{2+} complexes of PBT2 and its non-chlorinated homologue with Aβ$_{1–40}$ and other imidazole-bearing (N_{Im}) co-ligands. A detailed comparison with previously obtained parameters is shown in Table S1.

Complex	g_z	A_z (^{63}Cu) [a]	Reference
L = PBT2			
CuL	2.259 ± 0.002	151 ± 1	This work
CuL$_2$	2.283 ± 0.002	148 ± 3	This work
CuLN_{Im}^{X}			
X = Aβ$_{1–40}$	2.249 ± 0.002	147 ± 2	This work
X = imidazole	2.248 ± 0.001	143 ± 1	This work
X = histamine	2.248 ± 0.001	143 ± 1	This work
X = Aβ$_{1–42}$	2.242 ± 0.002	142 ± 3	10 [b]
L = non-chlorinated PBT2 homologue			
CuL	2.255 ± 0.001	153 ± 1	6
CuL$_2$	2.267 ± 0.001	149 ± 1	6
CuLN_{Im}^{X}			
X = imidazole	2.245 ± 0.001	144 ± 1	This work, 6, 11
X = histamine	2.245 ± 0.001	145 ± 1	This work, 6, 11
Aβ			
Cu(Aβ$_{1–40}$)	2.268 ± 0.002	174 ± 2	This work [c]
Cu$_2$(Aβ$_{1–40}$)			
first site	2.268 ± 0.002	174 ± 2	This work [d]
second site	2.309 ± 0.005	168 ± 5	This work [d]

[a] Hyperfine parameters are expressed in units of 10^{-4} cm^{-1} (1×10^{-4} cm^{-1} = 2.9979 MHz). To aid comparison with other studies, hyperfine couplings have been converted from those obtained using ^{65}Cu to those expected for ^{63}Cu using the scaling factor $|g_n(^{65}Cu) / g_n(^{63}Cu)| = 1.07$. [b] Species was not assigned to a ternary complex and spectral isolation was approximate. [c] Parameters are those for the dominant species at pH 7.4. [d] Parameters assume that the coordination of the first-bound ion ("first site") are the same as those for Cu(Aβ).

Table 2. Stepwise conditional formation constants (pH 7.4) used to simulate the species distributions of Cu/L/N_{Im}^{X} mixtures for X = Aβ$_{1–40}$ (Figure 2c), imidazole (Figure S6c), and histamine (Figure S9c). A detailed comparison of Cu^{2+} formation constants, including those for the non-chlorinated homologue of PBT2 and various N_{Im} donors, is provided in Table S2.

Complex	Formation constant [a]	log[${}^{c}K$ / (1 M^{-1})] at pH 7.4	Reference
CuL	${}^{c}K^{Cu}_{CuL}$	13.61 ± 0.05	8
CuL$_2$	${}^{c}K^{CuL}_{CuL_2}$	5.95 ± 0.07	8
CuL$N_{Im}^{A\beta}$ (His6)	${}^{c}K^{CuL}_{CuLN_{Im}^{H6}}$	6.4 ± 0.1	This work
CuL$N_{Im}^{A\beta}$ (His13/14)	${}^{c}K^{CuL}_{CuLN_{Im}^{H13/14}}$	4.4 ± 0.1	This work

Preprints (www.preprints.org) | NOT PEER-REVIEWED | Posted: 5 May 2023 doi:10.20944/preprints202305.0275.v1

$CuLN_{Im}^{imidazole}$	${}^{c}K^{CuL}_{CuLN_{Im}^{imidazole}}$	4.22 ± 0.09	This work
$CuLN_{Im}^{histamine}$	${}^{c}K^{CuL}_{CuLN_{Im}^{histamine}}$	4.00 ± 0.05	This work
$Cu(A\beta_{1–40})$	${}^{c}K^{Cu}_{Cu(A\beta)}$	10.0 ± 0.1	This work
$Cu_2(A\beta_{1–40})$	${}^{c}K^{Cu(A\beta)}_{Cu_2(A\beta)}$	8.0 ± 0.1	This work

[a] Formation constants are defined in Equations 2–4 (Section 4.3).

More than three Cu^{2+} ions cannot be accommodated by an equimolar PBT2/Aβ mixture, with the excess Cu^{2+} ions existing as aqueous copper that will precipitate as $[Cu(OH)_2]_n$ at pH 7.4. Inclusion of $Cu(PBT2)N_{Im}^{H13/14}$, whose formation does not depend on the Cu^{2+} loading state of Aβ, was essential to fit the experimental data. Alternative explanations of the physical origin of the lower-affinity ternary complex, such as a change in coordination of the first-bound Cu^{2+} ion in $Cu_2(A\beta)$, can be ruled out because the concentration of $Cu_2(A\beta)$ relative to that of the ternary complex is too low at $n < 2$ (Figure S5).

The fact that ${}^{c}K^{CuL}_{CuLN_{Im}^{H6}}$ is 100-fold larger than ${}^{c}K^{CuL}_{CuLN_{Im}^{H13/14}}$ indicates that either $Cu(PBT2)N_{Im}^{H6}$ is stabilized by favorable outer-sphere ligand–peptide interactions and/or that $Cu(PBT2)N_{Im}^{H13/14}$ is destabilized by such interactions. To distinguish between these possibilities, we repeated the EPR analyses using Cu/PBT2/X 1:1:*n* systems with relatively unstructured N_{Im} donor ligands from X = imidazole (Figures S6–S8) and histamine (Figures S9–S11). The EPR spectra of the isolated ternary $Cu(PBT2)N_{Im}^{X}$ complexes were characterized by the same parameters as $Cu(PBT2)N_{Im}^{A\beta}$ spectra (Table 1), confirming that each of these ternary Cu^{2+} complexes involves monodentate N_{Im} coordination of the co-ligand (Figure 1). The difference between ${}^{c}K^{CuL}_{CuLN_{Im}^{imidazole}}$ and ${}^{c}K^{CuL}_{CuLN_{Im}^{H13/14}}$ was within experimental error, whereas ${}^{c}K^{CuL}_{CuLN_{Im}^{histamine}}$ was slightly lower than these constants (Table 2). Thus, we may conclude that the stability of $Cu(PBT2)N_{Im}^{H13/14}$ is not strongly influenced by outer-sphere ligand–peptide interactions, whereas such interactions greatly enhance the stability of $Cu(PBT2)N_{Im}^{H6}$.

To independently verify the EPR method for deriving the conditional formation constants, we performed the same analyses for ternary complexes of the non-chlorinated homologue of PBT2 (L′) with imidazole (Figures S12–S14) and compared the value with that previously determined using potentiometric titrations [11]. After pH correction of the absolute stability constants (Table S3), ${}^{c}K^{CuL'}_{CuL'N_{Im}^{imidazole}}$ was not significantly different from that determined here using EPR (Table S2) and, similar to PBT2, slightly higher than ${}^{c}K^{CuL'}_{CuL'N_{Im}^{histamine}}$ (Figures S15–S17).

3. Discussion

EPR spectroscopy isolated a common $Cu(PBT2)N_{Im}^{A\beta}$ spectrum for (Figure S3) for both $Cu(PBT2)N_{Im}^{H6}$ and $Cu(PBT2)N_{Im}^{H13/14}$ because they have very similar first coordination spheres. Nevertheless, as has been shown for other terdentate Cu^{2+} chelators [27,28], ternary complexes with different N_{Im} donor ligands can be distinguished based on their distinct formation constants, which are determined by outer-sphere interactions to which continuous-wave EPR is typically insensitive. Importantly, the spectroscopic signature of $Cu(PBT2)N_{Im}^{A\beta}$ isolated here for Cu/PBT2/$A\beta_{1–40}$ *n*:1:1 closely matches that reported for the species isolated in Cu/PBT2/$A\beta_{1–42}$ 1:2:1 [10]. In the latter study, the authors ascribed this to a unique PBT2-inaccessible Cu(Aβ) complex and concluded that there was no evidence for ternary complex formation. However, we have shown that $CuLN_{Im}^{X}$ complexes with this spectroscopic signature are formed by PBT2 with a number of N_{Im} donor ligands X (Table 1, Table S1). Moreover, we demonstrated the requirement for two such complexes — $Cu(PBT2)N_{Im}^{H6}$ and $Cu(PBT2)N_{Im}^{H13/14}$ — with distinct stabilities (Table 2) to explain the species distributions of Cu/PBT2/$A\beta_{1–40}$ mixtures. The relatively high stability of $Cu(PBT2)N_{Im}^{H6}$ compared with complexes formed with other N_{Im} donors might result from stabilizing pi–pi stacking of the aromatic rings of PBT2 and Phe4 or Tyr10, although a combination of electrostatic, steric, and hydrogen-bonding effects may contribute.

Despite the large ternary formation constant for $Cu(PBT2)N_{Im}^{H6}$, PBT2 remains a promiscuous Cu^{2+} chelator because it is capable of forming a ternary $Cu(PBT2)N_{Im}$ complex with all N_{Im} donor ligands, including ubiquitous His side chains of peptides and proteins in the biological milieu, whose combined effect should outweigh that of a single $Cu(PBT2)N_{Im}^{A\beta}$ complex regardless of its stability. We therefore conclude that PBT2 is capable of accessing

Preprints (www.preprints.org) | NOT PEER-REVIEWED | Posted: 5 May 2023 doi:10.20944/preprints202305.0275.v1

Cu(Aβ) complexes with high stability but not specificity. Potential functional implications of Cu(PBT2)N_{Im} complexes have been discussed in our previous studies of the non-chlorinated PBT2 homologue. First, as an alternative to acting as a mobile ion carrier (ionophore) in a lipid membrane, endocytosis of extracellular proteins on which Cu(PBT2) is anchored, followed by release of Cu^{2+} in low-pH and/or reducing intracellular compartments, may contribute to bulk transport of these ions [6]. Second, their production of ROS in the presence of ascorbate [11], in addition to the modulation of cellular ROS signaling following exposure to this class of ligand [16], contrasts with the originally intended ROS-silencing of function of PBT2 [17].

Recently, PBT2 has found renewed interest as an antimicrobial compound. Notably, a number of gram-positive bacteria became re-sensitized to previously resistant classes of antibiotic when these antibiotics were supplemented with PBT2 and Zn^{2+} in mouse models of wound healing [18] and pneumonia [19]. These results have been attributed multiple bactericidal mechanisms associated with intracellular Zn^{2+} accumulation, including impairment of Mn-dependent superoxide dismutase and production of ROS [20]. Although ligands generally have a greater affinity for Cu^{2+} compared with Zn^{2+} [21], the above effects were observed in response to co-administration of PBT2 (~1 μM) with an excess of Zn^{2+} (~100 μM). Therefore, remains unclear whether ternary Cu(PBT2)N_{Im} complexes may be formed under these conditions. However, given the ability of PBT2 to also form terdentate Zn^{2+} chelates [7], the role of similar Zn(PBT2)N_{Im} complexes in the antimicrobial activity of Zn/PBT2 may be speculated.

4. Materials and Methods

4.1. Sample preparation

$A\beta_{1–40}$ (purity >95%) was synthesized in the Peptide Technology Facility of the Bio21 Molecular Science and Biotechnology Institute, The University of Melbourne. The lyophilised peptide was dissolved at a nominal concentration of 1 mg/mL in 1,1,1,3,3,3-hexafluoroisopropanol and portioned, then the solvent was allowed to evaporate. The resulting peptide film was resuspended at 4°C in 20% v/v 20 mM NaOH, 70% v/v ultrapure water (MilliQ, Merck), and 10% v/v 10× phosphate buffered saline (PBS; 10 mM phosphate buffer, 2.7 mM KCl, 137 mM NaCl; Sigma). After centrifugation at 14000×*g* for 15 min at 4°C, the supernatant was retained and the peptide concentration immediately determined using $\varepsilon_{214} = 74925\ M^{-1}cm^{-1}$ [22]. A concentrated stock of $^{65}CuCl_2$ was prepared by stirring ^{65}CuO (^{65}Cu, > 99%; Cambridge Isotope Laboratories) in concentrated HCl, evaporating excess HCl under heat, then adding ultrapure water. PBT2 was synthesized as previously described [23], and a 1mM stock solution was prepared by solubilising the hydrochloride salt directly in PBS.

From the above stock solutions, PBT2 and then $^{65}CuCl_2$ were added to portions of $A\beta_{1–40}$ to achieve final molar Cu/PBT2/ ratios of *n*:1:1 (*n* = 0.33–2.67) with [$A\beta_{1–40}$] = 200 μM. Control samples containing Cu/PBT2 0.5:1 and 1:1 and Cu/$A\beta_{1–40}$ 1:1 and 2.5:1 were also prepared. Glycerol (10% v/v) was added to the Cu/PBT2 control samples to prevent formation of a concentrated solute phase upon freezing. Immediately after Cu addition, the final solution pH was measured using a micro-probe (Hanna Instruments, Italy) and adjusted using concentrated NaOH or HCl as required. Samples were transferred to quartz EPR tubes (Wilmad, SQ-707) and snap frozen in liquid nitrogen within two minutes of Cu addition.

4.2. EPR spectroscopy

X-band continuous-wave EPR spectra were acquired using a Bruker ESP380E spectrometer fitted with a rectangular TE_{102} microwave cavity and a quartz cold finger insert. Microwave frequencies were measured using an EIP Microwave 548A frequency counter and *g* factors calibrated against the F^+ line in CaO ($g = 2.0001 \pm 0.0002$) [24]. Experimental conditions are indicated in the figure captions. Background correction was performed by subtraction of the buffer-only spectrum.

The "pepper" function in EasySpin v.5.2.33 [25,26] was used to simulate basis spectra using the static Hamiltonian

$$H = \beta_e \mathbf{B}^T \cdot \mathbf{g} \cdot \mathbf{S} + \mathbf{S}^T \cdot \mathbf{A} \cdot \mathbf{I} - g_n \beta_n \mathbf{B}^T \cdot \mathbf{I} \quad (1)$$

Preprints (www.preprints.org) | NOT PEER-REVIEWED | Posted: 5 May 2023 doi:10.20944/preprints202305.0275.v1

where **S** and **I** are the electron and ^{65}Cu nuclear vector spin operators, **g** and **A** are the 3×3 electron Zeeman and ^{65}Cu electron-nuclear hyperfine coupling matrices, β_e is the Bohr magneton, β_n is the nuclear magneton and B is the applied magnetic field vector. Rhombic symmetry or higher was assumed for **g** and **A**, with principal values of g_x, g_y, and g_z and A_x, A_y, and A_z, respectively. the Hamiltonian in equation 3. Assuming at least rhombic symmetry, the principal values of g and A and the lineshape parameters (g–A strain model) were varied iteratively using the "esfit" module in EasySpin to achieve a least squares minimization of the difference between the experimental and simulated spectra.

4.3. Determination of the ternary formation constants for Cu/PBT2/Aβ$_{1–40}$

The Cu(PBT2)N$_{Im}^{Aβ}$ species was assumed to arise from the superposition of two ternary complexes. The first complex involved anchoring of Cu(PBT2) on the His6 side chain (N$_{Im}^{H6}$), which is also required for Cu(Aβ) formation; the second involved anchoring on a side chain of either His13 or His14 (N$_{Im}^{H13/14}$), which is not required for Cu(Aβ) or Cu$_2$(Aβ) formation. Thus, Cu(Aβ) and Cu$_2$(Aβ) can simultaneously accommodate an Cu(PBT2)N$_{Im}^{H13/14}$ complex but not a Cu(PBT2)N$_{Im}^{H6}$ complex. Under these assumptions, Cu/PBT2/Aβ$_{1–40}$ n:1:1 can be modeled as Cu/L/A/B n:1:1:1, where ligand L is PBT2, ligand A acts like Aβ, and ligand B is treated an isolated N$_{Im}^{H13/14}$ donor. The relevant formation constants are

$$\begin{aligned}
\beta'_{1100} &= {}^{c}K^{Cu}_{CuL} && \text{for Cu(PBT2)}\\
\beta'_{1200} &= {}^{c}K^{Cu}_{CuL} \times {}^{c}K^{CuL}_{CuL_2} && \text{for Cu(PBT2)}_2\\
\beta'_{1010} &= {}^{c}K^{Cu}_{CuA} && \text{for Cu(Aβ)}\\
\beta'_{1020} &= {}^{c}K^{Cu}_{CuA} \times {}^{c}K^{CuA}_{Cu_2A} && \text{for Cu}_2\text{(Aβ)}\\
\beta'_{1110} &= {}^{c}K^{Cu}_{CuL} \times {}^{c}K^{CuL}_{CuLA} && \text{for Cu(PBT2)N}_{Im}^{H6}\\
\beta'_{1101} &= {}^{c}K^{Cu}_{CuL} \times {}^{c}K^{CuL}_{CuLB} && \text{for Cu(PBT2)N}_{Im}^{H13/14}.
\end{aligned} \quad (2)$$

where the cumulative conditional (pH-dependent) constants (β') are defined by

$$\beta'_{pqrs} = \frac{[Cu_pL_qA_rB_s]}{[Cu]^p[L]^q[A]^r[B]^s} \quad \text{for} \quad pCu + qL + rA + sB \overset{\beta_{pqrs}}{\rightleftharpoons} Cu_pL_qA_rB_s \quad (3)$$

and the stepwise conditional formation constants (${}^{c}K$) are defined by

$$\begin{aligned}
{}^{c}K^{Cu}_{CuX} &= \frac{[CuX]}{[Cu][X]} && \text{for} \quad Cu + X \overset{{}^{c}K^{Cu}_{CuX}}{\rightleftharpoons} CuX \quad (X = L, A)\\
{}^{c}K^{CuL}_{CuLX} &= \frac{[CuLX]}{[CuL][X]} && \text{for} \quad CuL + X \overset{{}^{c}K^{CuL}_{CuLX}}{\rightleftharpoons} CuLX \quad (X = A, B)\\
{}^{c}K^{CuA}_{Cu_2A} &= \frac{[Cu_2A]}{[CuA][Cu]} && \text{for} \quad CuA + Cu \overset{{}^{c}K^{CuA}_{Cu_2A}}{\rightleftharpoons} Cu_2A.
\end{aligned} \quad (4)$$

To determine the ternary formation constants ${}^{c}K^{CuL}_{CuLA}$ and ${}^{c}K^{CuL}_{CuLB}$, we made use of the previously publishes values for ${}^{c}K^{Cu}_{CuL}$, ${}^{c}K^{CuL}_{CuL_2}$, ${}^{c}K^{Cu}_{CuA}$ and ${}^{c}K^{CuA}_{Cu_2A}$ at pH 7.4 (Table 2, Table S2), then initial guesses for ${}^{c}K^{CuL}_{CuLA}$ and ${}^{c}K^{CuL}_{CuLB}$ were made and their values systematically varied as follows:

1) For each value of ${}^{c}K^{CuL}_{CuLA}$ and ${}^{c}K^{CuL}_{CuLB}$, the theoretical distributions of CuL, CuL$_2$, CuA, Cu$_2$A, CuLA, and CuLB were calculated for the condition Cu/PBT2/Aβ$_{1–40}$ 1:1:1 ≡ Cu/L/A/B 1:1:1:1 under which spectral features attributable to the ternary species were maximal (Figure 2c);

2) The theoretical speciation in step 1 provided weighting factors that were used to algebraically subtract the normalized spectra of CuL, CuL_2, and CuA (Figure 2b) from the experimental spectrum of Cu/PBT2/$A\beta_{1-40}$ 1:1:1 ≡ Cu/L/A/B 1:1:1:1, thus yielding a weighted summation of indistinguishable CuLA and CuLB spectra;

3) Linear combinations of the normalized CuL, CuL_2, CuA, Cu_2A, CuLA, CuLB basis spectra were used to reconstruct the experimental EPR spectra at all intermediate stoichiometries Cu/PBT2/$A\beta_{1-40}$ n:1:1 ≡ Cu/L/A/B n:1:1:1 ($0.33 \leq n \leq 2.67$), the weightings being iteratively varied using a generalized reduced gradient nonlinear solver (Frontline Systems, Inc., www.solver.com) to minimize the root-mean-squared deviation between the reconstructions and the experimental spectra;

4) The deviation between the fitted and experimental values of [CuL], [CuL_2], [CuA], [Cu_2A], and [$CuLN_{Im}^{A\beta}$] = [CuLA] + [CuLB] for all values of n was calculated;

5). New values of ${}^{c}K_{CuLA}^{CuL}$ and ${}^{c}K_{CuLB}^{CuL}$ were chosen and steps 1–4 repeated until the root-mean-squared deviation was minimised.

The above method assumed that the frozen-solution EPR spectra of Cu(PBT2)N_{Im}^{H6} and Cu(PBT2)$N_{Im}^{H13/14}$ are indistinguishable, which is justified by the identification of a common set of spin Hamiltonian parameters for numerous Cu(PBT2)N_{Im} complexes with different N_{Im} donor ligands (Table 1, Tale S1). This assumption was also shown to be true for ternary Cu^{2+} complexes of different N_{Im} donors with other terdentate ligands such as the non-chlorinated homologue of PBT2 (Table S1), the GHK tripeptide [27,28], and α-synuclein [29].

Supplementary Materials: The following supporting information can be downloaded at: www.mdpi.com/xxx/s1, Figures S1–S17; Tables S1–S3; Equations S1–S5.

Funding: This research received no external funding.

Data Availability Statement: The data presented in this study are available on request from the corresponding author.

Acknowledgments: The support of the Brain–Immune Communication laboratory, Institute Pasteur is gratefully acknowledged. PBT2 was kindly supplied by Dr Vijaya Kenche, Florey Institute of Neuroscience and Mental Health, Australia.

Conflicts of Interest: The author declares no conflict of interest.

Reference

1. Bush, A.I. Metals and neuroscience. *Curr. Opin. Chem. Biol.* **2000**, *4*, 184–191. doi: 10.1016/S1367-5931(99)00073-3.
2. Bush, A.I. Drug development based on the metals hypothesis of Alzheimer's disease. *J. Alzheimers Dis.* **2008**, *15*, 223–240. doi: 10.3233/JAD-2008-15208.
3. Adlard, P.A.; Bica, L.; White, A.R.; Nurjono, M.; Filiz, G.; Crouch, P.J.; Donnelly, P.S.; Cappai, R.; Finkelstein, D.I.; Bush, A.I. Metal ionophore treatment restores dendritic spine density and synaptic protein levels in a mouse model of Alzheimer's disease. *PLoS ONE* **2011**, 6, e17669. doi: 10.1371/journal.pone.0017669.
4. Sampson, E.L.; Jenagaratnam, L.; McShane, R. Metal protein attenuating compounds for the treatment of Alzheimer's dementia. *Cochrane Database Syst. Rev.* **2014**, CD005380. doi: 10.1002/14651858.CD005380.pub5.
5. www.alzforum.org/news/research-news/pbt2-takes-dive-phase-2-alzheimers-trial (1 April 2014).
6. Kenche, V.B.; Zawisza I.; Masters, C.L.; Bal, W.; Barnham, K.J.; Drew, S.C. Mixed ligand Cu^{2+} complexes of a model therapeutic with Alzheimer's amyloid-β peptide and monoamine neurotransmitters. *Inorg. Chem.* **2013**, 52, 4303–4318. doi: 10.1021/ic302289r.
7. Nguyen, M.; Vendier, L.; Stigliani, J-L., Meunier, B.; Robert, A. Structures of the Copper and Zinc Complexes of PBT2, a Chelating Agent Evaluated as Potential Drug for Neurodegenerative Diseases. *Eur. J. Inorg. Chem.* **2017**, 600–608. doi: 10.1002/ejic.201601120.
8. Sgarlata, C.; Arena, G.; Bonomo, R.P.; Giuffrida, A.; Tabbì, G. Simple and mixed complexes of copper(II) with 8-hydroxyquinoline derivatives and amino acids: Characterization in solution and potential biological implications. *J. Inorg. Biochem.* **2018**, *180*, 89–100. doi: j.jinorgbio.2017.12.002.

9. Summers, K.L.; Roseman, G.P.; Sopasis, G.J.; Millhauser, G.L.; Harris, H.H.; Pickering, I.J.; George, G.N. Copper(II) Binding to PBT2 Differs from That of Other 8-Hydroxyquinoline Chelators: Implications for the Treatment of Neurodegenerative Protein Misfolding Diseases. *Inorg. Chem.* **2020**, *59*, 17519–17534. doi: 10.1021/acs.inorgchem.0c02754.
10. Summers, K.L.; Roseman, G.; Schilling, K.M.; Dolgova, N.V.; Pushie, M.J.; Sokaras, D.; Kroll, T.; Harris, H.H.; Millhauser, G.L.; Pickering, I.J.; George, G.N. Alzheimer's Drug PBT2 Interacts with the Amyloid β 1–42 Peptide Differently than Other 8-Hydroxyquinoline Chelating Drugs. *Inorg. Chem.* **2022**, *61*, 14626–14640. doi: 10.1021/acs.inorgchem.2c01694.
11. Mital, M.; Zawisza, I.A.; Wiloch, M.Z.; Wawrzyniak, U.E.; Kenche, V.; Wróblewski, W.; Bal, W.; Drew, S.C. Copper Exchange and Redox Activity of a Prototypical 8-Hydroxyquinoline: Implications for Therapeutic Chelation. *Inorg Chem.* **2016**, *55*, 7317–7319. doi: 10.1021/acs.inorgchem.6b00832.
12. Drew, S. C.; Barnham, K. J. The Heterogeneous Nature of Cu2+ Interactions with Alzheimer's Amyloid-β Peptide. *Acc. Chem. Res.* **2011**, *44*, 1146–1155. doi: 10.1021/ar200014u.
13. Faller, P.; Hureau, C.; La Penna, G. Metal ions and intrinsically disordered proteins and peptides: from Cu/Zn amyloid-β to general principles. *Acc. Chem. Res.* **47**, 2252–2259. doi: 10.1021/ar400293h.
14. Drew, S.C.; Noble, C.J.; Masters, C.L.; Hanson, G.R.; Barnham, K.J. Pleomorphic copper coordination by Alzheimer's amyloid-β peptide. *J. Am. Chem. Soc.* **2009**, *131*, 1195–1207. doi: 10.1021/ja808073b.
15. Alies, B.; Renaglia, E.; Rózga, M.; Bal, W.; Faller, P.; Hureau, C. Cu(II) affinity for the Alzheimer's peptide: tyrosine fluorescence studies revisited. *Anal. Chem.* **2013**, *85*, 1501–1508. doi: 10.1021/ac302629u.
16. Haigh, C.L.; Tumpach, C.; Collins, S.J.; Drew, S.C. A 2-substituted 8-hydroxyquinoline stimulates neural stem cell proliferation by modulating ROS signalling. *Cell Biochem. Biophys.* **2016**, *74*, 297–306. doi: 10.1007/s12013-016-0747-4.
17. Drew, S.C. The case for abandoning therapeutic chelation of copper ions in Alzheimer's disease. *Front. Neurosci.* **2017**, *11*, 317. doi: 10.3389/fnins.2017.00317.
18. Bohlmann, L.; De Oliveira, D.M.P.; El-Deeb, I.M.; Brazel, E.B.; Harbison-Price, N.; Ong, C.Y.; Rivera-Hernandez, T.; Ferguson, S.A.; Cork, A.J.; Phan, M.D.; Soderholm, A.T.; Davies, M.R.; Nimmo, G.R.; Dougan, G.; Schembri, M.A.; Cook, G.M.; McEwan, A.G.; von Itzstein, M.; McDevitt, C.A.; Walker, M.J. Chemical Synergy between Ionophore PBT2 and Zinc Reverses Antibiotic Resistance. *mBio*. **2018**, *9*, e02391-18. doi: 10.1128/mBio.02391-18.
19. Brazel, E.B.; Tan, A.; Neville, S.L.; Iverson, A.R.; Udagedara, S.R.; Cunningham, B.A.; Sikanyika, M.; De Oliveira, D.M.P.; Keller, B.; Bohlmann, L.; El-Deeb, I.M.; Ganio, K.; Eijkelkamp, B.A.; McEwan, A.G.; von Itzstein, M.; Maher, M.J.; Walker, M.J.; Rosch, J.W.; McDevitt, C.A. Dysregulation of Streptococcus pneumoniae zinc homeostasis breaks ampicillin resistance in a pneumonia infection model. *Cell Rep*. **2022**, *38*, 110202. doi: 10.1016/j.celrep.2021.110202.
20. Harbison-Price, N.; Ferguson, S.A.; Heikal, A.; Taiaroa, G.; Hards, K.; Nakatani, Y.; Rennison, D.; Brimble, M.A.; El-Deeb, I.M.; Bohlmann, L.; McDevitt, C.A.; von Itzstein, M.; Walker, M.J.; Cook, G.M. Multiple Bactericidal Mechanisms of the Zinc Ionophore PBT2. *mSphere*. **2020**, *5*, e00157-20. doi: 10.1128/mSphere.00157-20.
21. Irving, H.; Williams, R.J.P. The stability of transition-metal complexes. *J. Chem. Soc.* **1953**, 3192–3210.
22. Kuipers, B.J.H.; Gruppen, H. Prediction of Molar Extinction Coefficients of Proteins and Peptides Using UV Absorption of the Constituent Amino Acids at 214 nm To Enable Quantitative Reverse Phase High-Performance Liquid Chromatography-Mass Spectrometry Analysis. *J. Agric. Food Chem.* **2007**, *55*, 5445–5451. doi: 10.1021/jf070337l.
23. Barnham, K.J.; Gautier, E.C.L.; Kok, G.B.; Krippner, G. Preparation of 8-hydroxyquinolines for treatment of neurological conditions. 2008. U.S. Pat. Appl. Publ. Patent version number 20080161353 A1, United States.
24. Wertz, J.E.; Orton, J.W.; Auzins, P. Electron spin resonance studies of radiation effects in inorganic solids. *Discuss. Faraday Soc*. **1961**, *31*, 140–150. doi: 10.1016/j.ijpharm.2003.07.002.
25. Stoll, S.; Britt, R.D. General and efficient simulation of pulse EPR spectra. *Phys. Chem. Chem. Phys.* **2009**, *11*, 6614–6625. doi: 10.1039/b907277b.
26. Stoll, S.; Schweiger, A. EasySpin, a comprehensive software package for spectral simulation and analysis in EPR. *J. Magn. Reson.* **2006**, *178*, 42–55. doi: 10.1016/j.jmr.2005.08.013.
27. Bossak-Ahmad, K.; Wiśniewska, M.; Bal, W.; Drew, S.C.; Frączyk, T. Ternary Cu(II) complex with GHK peptide and cis-urocanic acid as a potential physiologically functional copper chelate. *Int. J. Mol. Sci.* **2020**, *21*, 6190.
28. Bossak-Ahmad, K.; Bal, W.; Frączyk, T.; Drew, S.C. Ternary Cu^{2+} Complexes of Human Serum Albumin and Glycyl-L-histidyl-L-lysine. *Inorg. Chem.* **2021**, *60*, 16927–16931.
29. Drew, S.C. α-synuclein and β-amyloid form a bridged copper complex. *Appl. Magn. Reson.* **2015**, *46*, 1041–1052.